H. Huang
K. C. Kiddy
Naval Surface Warfare Center
Indian Head Division
White Oak,
Silver Spring, MD 20903-5000

Transient Interaction of a Spherical Shell with an Underwater Explosion Shock Wave and Subsequent Pulsating Bubble

The nonlinear interaction problem is analyzed by simultaneously solving the mass, momentum, and energy conservation equations together with appropriate material constitutive equations governing the fluid dynamics of the explosion gaseous product and the water and the structural dynamics of the compliant shell. A finite difference technique in a coupled Eulerian–Lagrangian scheme is used. The computer program PISCES 2DELK is employed to carry out the numerical computations. The results demonstrate that to rigorously analyze the response of a submerged structure to a nearby explosion, the interactions among the explosion shock wave, the structure, its surrounding media, and the explosion bubble need to be considered. © *1995 John Wiley & Sons, Inc.*

INTRODUCTION

Immediately after an explosive charge is detonated underwater, the solid explosive material is converted into high pressure gaseous reaction products. This high pressure is transmitted into the surrounding water and propagates therein as a shock wave generally referred to as the underwater explosion initial shock wave. The high pressure gaseous product, referred to as the gas globe or the bubble, expands rapidly against the ambient water until the gas pressure has fallen substantially below the ambient pressure. Then the bubble contracts due to the higher surrounding pressure and recompresses the gaseous product. Near the instant when the bubble reaches its minimum volume, a secondary pressure pulse, also referred to as the bubble pulse, is emitted. The bubble pulsates in this manner several times, except for near surface explosions where the bubbles are vented early. The dynamic behavior of the bubble is strongly influenced by the gravity field and the surrounding flow field and therefore the nearby boundary conditions such as presented by the free surface, the bottom, and the shape and motion of a structure. A rigid surface attracts and the free surface repels the bubble. Gravity causes the bubble to migrate upward. If there is a sufficient difference in pressure between opposite sides of the contracting bubble, the higher pressure side is pushed inward faster than the lower pressure side, the bubble assumes a kidneylike shape; subsequently the two interfaces impinge upon each other and the bubble becomes

Received November 10, 1994; Accepted June 6, 1995
Shock and Vibration, Vol. 2, No. 6, pp. 451–460 (1995)

CCC 1070-9622/95/060451-10

a torus. This induces a high velocity water jet penetrating through the torus. An excellent compact and comprehensive description of the hydrodynamics of the underwater explosion shock wave and bubble was published by Snay (1957). For a detailed exposition of the subject, the reader is referred to the classical text of Cole (1948).

A submerged structure nearby the explosion will be first impinged upon by the initial shock wave and subsequently also subjected to the bubble pulse loading, the dynamic loading due to the pulsating bubble flow field, as well as—depending on the standoff, orientation, and depth of the explosion—the impact of the bubble jet. In the energy partition of an underwater explosion, about 50% of the total energy of the charge is radiated in the initial shock wave and the other 50% is found in the energy of the bubble (Snay, 1957). Therefore, the bubble loading, vis-à-vis the initial shock wave, can be expected to contribute significantly to the damage of the structure.

Past studies of structural response to underwater explosions (Keil, 1961; Geers, 1975) have shown that during the action of the initial shock wave there is a strong interdependence between the actual loading acting on the structure and the structural response. For the case where the bubble is sufficiently far away from the structure, the bubble–structure interaction is insignificant and can be neglected (Hicks, 1986). However, if the bubble is at the immediate proximity of the structure, as explained previously, its dynamic behavior including the collapse, the emission of the bubble pulse, and the formation of the bubble jet are strongly influenced by the structure and the structural motions. To rigorously determine the structural response to a nearby underwater explosion, it is necessary to first simultaneously solve the problem of scattering of the initial shock wave by the structure and the initial structural dynamic response problem and subsequently to simultaneously solve the hydrodynamics problem of the pulsating bubble and the later structural dynamic response problem. This article describes such a study for the response of a submerged spherical shell using modern computation methodology for continuum mechanics.

DESCRIPTION OF PROBLEM

The spherical shell and the spherical explosive charge are submerged at such depths that the free surface and the ocean bottom have no effect on the loading and response. The line joining the centers of the shell and the explosive is parallel to the gravity vector and the problem is thus axisymmetric with respect to this line. The standoff of the detonation from the shell is such that the explosion bubble will intersect and interact with the shell.

The detonation of the spherical charge is initiated at its center and ideal detonation is assumed. At the time equal to the radius of the charge divided by its detonation velocity, the solid explosive is completely converted into high temperature and high pressure gaseous products. The dynamic pulsation of the gas globe, the bubble, can be described by the conservation principles of mass, momentum, and energy of gas dynamics together with an appropriate equation of state. Likewise, the propagation of the shock wave and the bubble pulse in water and the dynamic motion of the water are governed by the conservation principles of hydrodynamics and the equation of state for water. The dynamic response of the spherical shell can be calculated using an elastoplastic shell theory taking into account both the geometric and the material nonlinearities. In the present study, the material viscosities in the explosion gaseous product and the water, damping in the shell, as well as all heat transfer effects are neglected. The interaction among the shell, its surrounding water, the nearby gas bubble, the incident shock wave, and the bubble pulse can be analyzed in detail by solving these equations simultaneously. This can be carried out using modern finite element/difference computation methodology for continuum mechanics.

Computation methods formulated in the Eulerian scheme, where the material moves through the computational mesh fixed in space, are well suited for the bubble pulsation, collapse, and the bubble jet formation (Tipton et al., 1991). Methods formulated in the Lagrangian scheme, where the computational mesh moves with the material, are well suited for the dynamic deflection of shells. Therefore, the present highly nonlinear problem needs to be analyzed in a coupled Eulerian–Lagrangian or an arbitrary Lagrangian–Eulerian formulation. A finite difference computer program named PISCES 2DELK (Hancock, 1987) for solving these conservation equations is employed to carry out the required computation here. This program possesses a coupled Eulerian–Lagrangian capability, equipped with Lagrangian elastoplastic shell elements and uses a

second-order accurate advection algorithm in its Eulerian computation.

PISCES FINITE DIFFERENCE MESH

Figure 1 is a close-up of the computational mesh for the vicinity of the spherical shell and the spherical charge prior to detonation. The gravitation vector points to the left. The shaded rectangle contains the Eulerian mesh fixed in space. The spherical shell is divided into Lagrangian axisymmetric shell segments being embedded in the Eulerian mesh to facilitate coupled Lagrangian–Eulerian computation. The meridian of the shell is represented in the figure by the larger circle and the Lagrangian shell mesh cannot be shown clearly. Initially the spherical shell contains a vacuum. The initial boundary of the spherical charge is denoted by the smaller circle. The charge is embedded in the Eulerian mesh. Water occupies the rest of the mesh exterior to the shell and the explosive charge. During dynamic motion and deflection, the Lagrangian shell mesh cuts across some portion of the Eulerian mesh. The coupled Lagrangian–Eulerian algorithm will activate these crosscut Eulerian elements and adjust their material contents to either water or gaseous product or vacuum according to the physical situation.

It is known that the Lagrangian mesh is computationally more efficient than the Eulerian mesh. Therefore it is both economical and appropriate to use Lagrangian mesh for regions where large mesh distortions are not expected. For the present problem, it is computationally more efficient to use Lagrangian mesh for regions sufficiently far away from the fully expanded bubble. Figure 1 shows the Lagrangian mesh outside and the overlapping Lagrangian mesh inside the shaded rectangle. The inner boundary of the Lagrangian

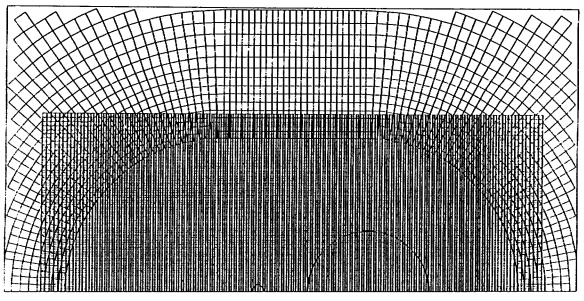

FIGURE 1 Close-up of the initial computation mesh.

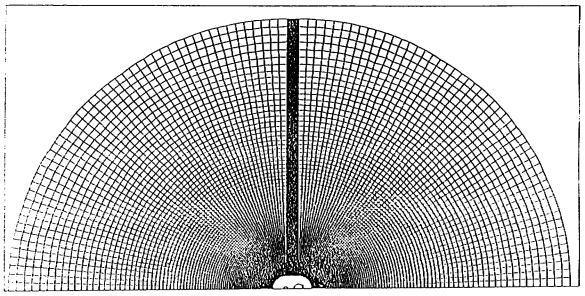

FIGURE 2 Entire initial computational mesh.

mesh is the arc near the perimeter of the rectangle. Again, the overlapping Lagrangian mesh is to facilitate coupled Lagrangian–Eulerian computation. The outer boundary of the Lagrangian mesh, i.e., the extent of the water included in the computation, depends on the problem requirements. The computational effort could be minimized by including an optimum extent of the water and invoking a nonreflecting or transmitting boundary condition at the outer boundary of the Lagrangian mesh. For the present 2-dimensional problem, a large mesh is used to insure that no reflection from the outer mesh boundary affects the solution for one bubble pulsation period. Figure 2 sketches the entire computational mesh prior to detonation. The dark areas therein are caused by the highly dense meshing used for those areas. For convenience, the present analysis uses a fixed boundary condition for the outer boundary of the Lagrangian mesh.

NUMERICAL RESULTS AND DISCUSSION

Computations are carried out for the case of the detonation of a spherical TNT charge underneath a steel spherical shell. The center of the charge is submerged at a depth of 304.8 m (1,000 ft) while the center of the shell is at 295.50 m (969.54 ft). The solid charge has a radius of 0.575 m and a weight of 1298 kg (2862 lb). The middle surface radius and thickness of the shell are 5.08 m (200 in.) and 0.1016 m (4 in.), respectively. It can be estimated using empirical formulas of underwater explosion (Keil, 1961) that the maximum bubble radius resulting from the free field detonation of this charge at this depth is 5.6 m and the duration of the first bubble pulsation is 0.187 s. To capture the significant interaction phenomena between

the bubble and the shell, the computation needs be carried out beyond 0.187 s.

The solid TNT charge has a density of 1630 kg/m^3 and a detonation velocity of 6930 m/s. The charge is detonated at its center at time $t = 0$. The detonation wave arrives at the surface of the charge at $t = 8.297 \times 10^{-5}$ s. At this time, the entire charge has been converted into gaseous product and the bubble begins to expand against the surrounding water. For the analysis of the gas dynamic behavior of the bubble, standard properties and the JWL equation of state for the TNT explosion product (Dobratz, 1981) are used. The shell is made of high strength steel with a yield stress equal to 919.80×10^6 N/m^2 (133,400 psi). Its density, Young's modulus, and Poisson's ratio are, respectively, 7893 kg/m^3, 206.843×10^9 N/m^2, and 0.3. For the present analysis of its large inelastic deformation, the Johnson–Cook constitutive model (Johnson and Cook, 1983), which also includes strain rate and temperature effects, is used. The water is treated as a compressible fluid with an initial density of 1000 kg/m^3. In the present PISCES computation, the polynomial equation of state for water is used. The cavitation pressure is set at 0.0 Pa. The Lagrangian shell mesh consists of 40 shell segments (axisymmetric elements). There are a total of 13,328 Eulerian zones (elements) and 7,884 Lagrangian zones in the entire computational mesh. In the shaded area and below the arc demarcating the outer Lagrangian zones in Fig. 1, the dimensions of an Eulerian zone are 0.2×0.2 m. The zone sizes increase gradually toward the outer boundary of the entire mesh. For the present computations, the radius of the outer Lagrangian mesh boundary is set to be 300 m to ensure that the reflection from this boundary does not arrive at the region of interest for the time duration of about two periods of the bubble pulsation. PISCES 2DELK uses an explicit method (the central difference method) for integrating the conservation equations forward in time. The time step used is less than the time it takes a stress wave to travel the length of the smallest element in the computational mesh. For numerical accuracy and stability, the computer program has built-in algorithms for automatic time step control (Hancock, 1987).

Interaction of a Fixed Rigid Sphere and the Explosion

To delineate the effects of the dynamic motions and deformations of the shell on the shell–bubble interaction, a computation is first carried out for the case in which the present shell is rigid and immovable while being subjected to the same described explosion. Figure 3 is a velocity vector plot for the fluid media at $t = 2.039 \times 10^{-3}$ s and infers that the initial spherical shock wave has just impinged upon the fixed sphere. The incident wave front pressure there is 1.53753×10^8 Pa (22,300 psi), a rather strong shock wave, as calculated by the empirical formula for TNT (Keil, 1961). The double horizontal lines appearing inside the smaller rectangle indicate the joining of the two Euler subgrids and have no effect on the numerical solution. Two subgrids are used because of limitations on the number of computational zones allowed per Euler subgrid. Therefore the double horizontal lines have no meaning in this and many of the subsequent figures. Figure 4 plots the time history of the volume of the explosion gaseous product and indicates that the bubble attains its maximum size at $t = 0.094$ s and is recompressed to its first minimum volume at $t = 0.199$ s. The first pulsation of the bubble has a period 0.012 s longer than that of the free field explosion. Figure 5 depicts the form of the bubble at $t = 0.100$ s intersecting the fixed sphere. Then the bubble volume decreases slightly from its maximum value and the pressure inside the bubble falls substantially below the ambient. In contrast to a free-field bubble, only the portion of the bubble surface not intersecting with the fixed sphere is being pushed back by the surrounding water, i.e., less force is applied for the recompression. This could explain why the first pulsation period of the bubble in this case is longer than that of a free field explosion. During this contraction, the bubble remains attached to the fixed sphere. Figure 6 shows the torus shaped bubble near its minimum at $t = 0.200$ s. From the plot of momentum vectors at $t = 0.200$ s of Fig. 7, it

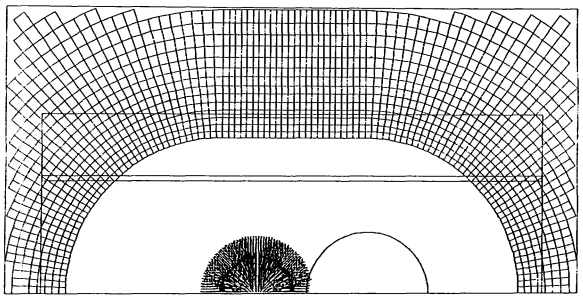

FIGURE 3 Velocity vector plot showing the initial shock wave impinging upon the fixed sphere.

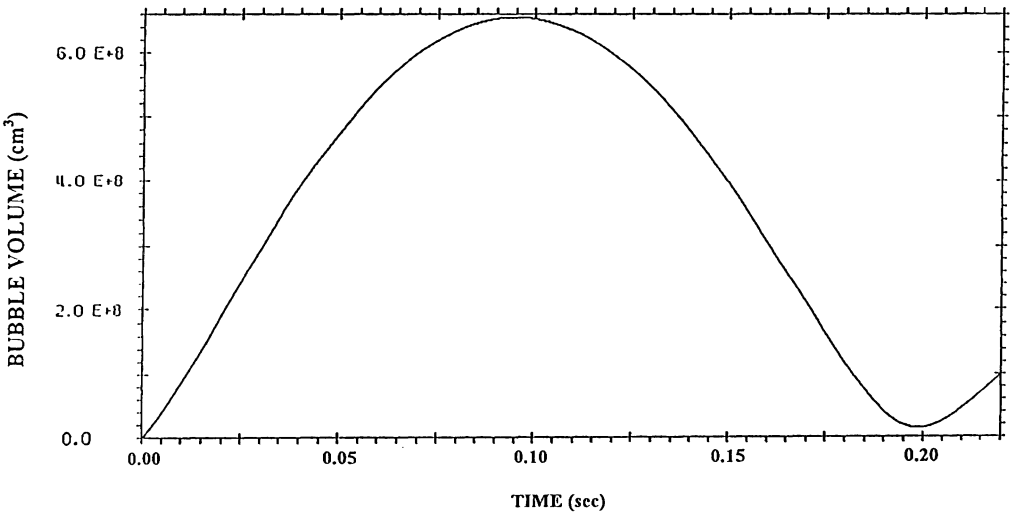

FIGURE 4 Time history of the volume of the bubble intersecting the fixed sphere.

can be seen that a strong water jet has been formed, penetrating through the torus and impacting the fixed sphere. From the magnitude of the momentum vector, it is estimated that the velocity of the water jet impacting the apex of the sphere is 350 m/s (1,150 ft/s). Figure 8 plots the shape of the reexpanding torus bubble at $t = 0.220$ s. Figure 9 plots the time history of pressure at the apex of the fixed sphere first impinged upon by the initial shock wave, contacted by the expanding bubble, and impacted by the bubble jet. The significant loadings on the sphere are those

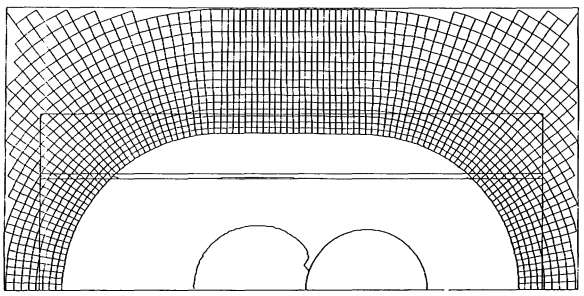

FIGURE 5 Bubble shape at 0.100 s, near its maximum volume and attaching to the fixed sphere.

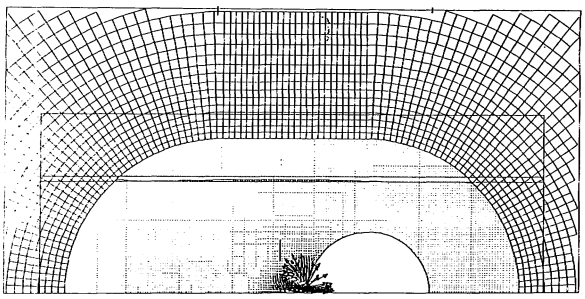

FIGURE 7 Momentum vector plot showing the water jet impacting the fixed sphere at 0.200 s.

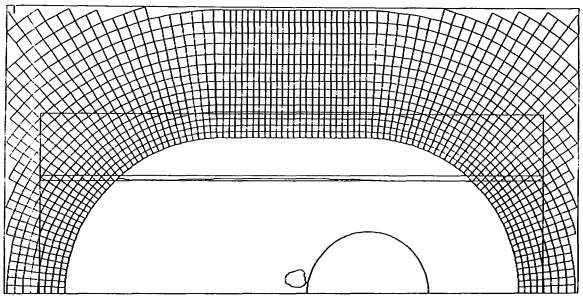

FIGURE 6 Bubble shape at 0.200 s, near its minimum volume and attaching to the fixed sphere.

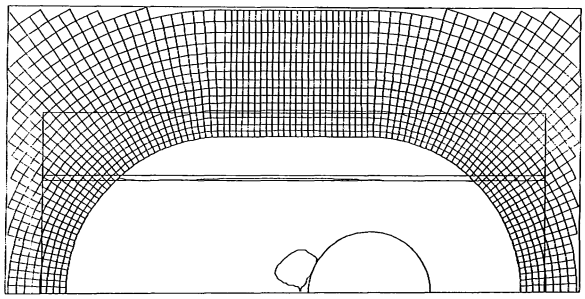

FIGURE 8 Reexpansion of the torus bubble attaching to the fixed sphere at 0.220 s.

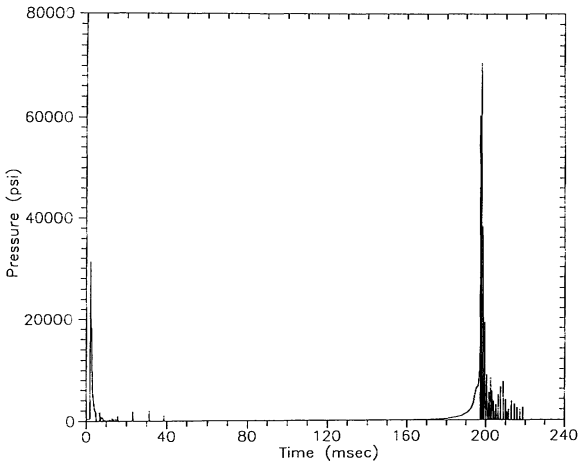

FIGURE 9 Pressure at the apex of the fixed sphere facing the explosion.

due to the initial shock wave, the reflection and diffraction thereof, the bubble jet impact, and the bubble pulse. The significant bubble loadings are separated from the shock wave loadings by a time span roughly equal to the period of the first bubble pulsation. The initial water jet impact pressure can be estimated by the water hammer equation (Plesset and Chapman, 1971) that states that on a rigid surface it is equal to the product of the water density multiplied by the water sound speed and the jet velocity. Based on the estimated jet velocity of 350 m/s (1,150 ft/s), the initial jet impact pressure is 5.75727×10^8 Pa (74,800 psi). The bubble loadings in Fig. 9 contain a very short duration high magnitude spike of 4.89527×10^8 Pa (71,000 psi) due to the water jet impact and agrees closely with the water hammer equation estimation. These numerical results demonstrate that the computation methodology is robust and capable of rendering detailed results representing the physics of the problem and agreeing very well with the deduction from experimental observations summarized in Cole (1948) and Snay (1957).

Interaction of an Unrestrained Steel Spherical Shell and the Explosion

Numerical results are then obtained for the case of the unrestrained steel shell subjected to the same explosion. Because the present article purports primarily to study the interaction effects, the hydrostatic prestress and the buoyancy effects of the shell are not included in the computation. The initial shock wave front impinges upon the spherical shell at the same time as the previous

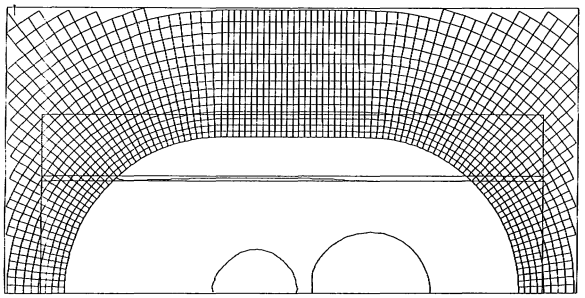

FIGURE 10 Bubble shape and shell deformation at 0.020 s.

case of a rigid and fixed sphere. As expected, there is no difference in the results for the two cases up to this time. Figure 10 shows the shapes of the expanding bubble and the deforming shell at $t = 0.020$ s. It can be seen that the effect of the initial shock wave results in a shell dimple which is 0.26 m (10.2 in.) deep at this time. At $t = 0.040$ s, as portrayed in Fig. 11, the depth of the dimple has increased to 0.296 m (11.65 in.) and the pressure waves reflected and radiated by the shell flatten the opposing surface of the expanding bubble at this instant. From then on until near the time when the bubble contracts to its minimum size, the dimple depth remains roughly at this magnitude. This implies that during this time span, the shell moves primarily in the rigid body mode, being pushed by the expanding bubble and sucked back by the contracting bubble. The shell response motion causes the pulsating bubble to assume different shapes than those for the previous fixed sphere case at corresponding times. The time histories of the upward deflections of the two apexes of the shell are plotted in Fig. 12 where A designates the apex first impinged upon and B the other apex on the far side.

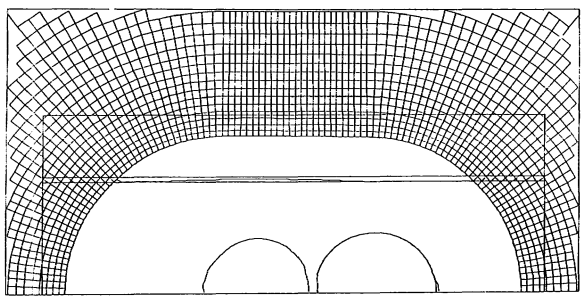

FIGURE 11 Bubble shape and shell deformation at 0.040 s.

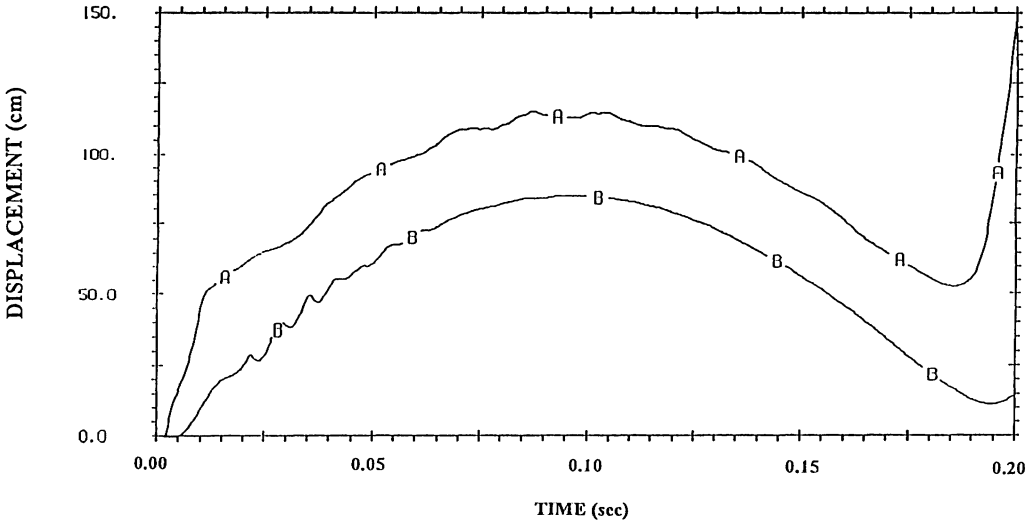

FIGURE 12 Time histories of shell deflections, A designates the front apex and B the rear apex.

The time histories of the upward velocities of these two apexes are plotted in Fig. 13. The early time velocity (the kickoff velocity) of apex A can be estimated by the simple linear theory of the response of a vacuum backed rigid plate of infinite extent impinged upon by a plane underwater shock wave (Keil, 1961). Using the maximum pressure and the exponential decay constant of the shock wave of the present explosion calculated by the empirical formulas for TNT (Keil, 1961), the early time velocity of apex A is also calculated by this plate theory and a linear theory of transient interaction of spherical incident waves with a spherical elastic shell (Huang et al., 1971). The results are compared to the nonlinear PISCES calculation in Fig. 14. The kickoff velocities agree within 10%. Because a relatively coarse mesh is used in the PISCES calculation, it is not expected that the shock wave front could be well represented when it impinges on the shell. The agreement on the kickoff velocity is indicative that the PISCES result nevertheless gives a correct initial impulse imparted to the shell by the shock wave, which is important for the prediction of structural damage. Figure 15 shows that at $t = 0.060$ s a small part of the expanding bubble protrudes out and touches the shell. Tracking the time history of the volume of the explosion prod-

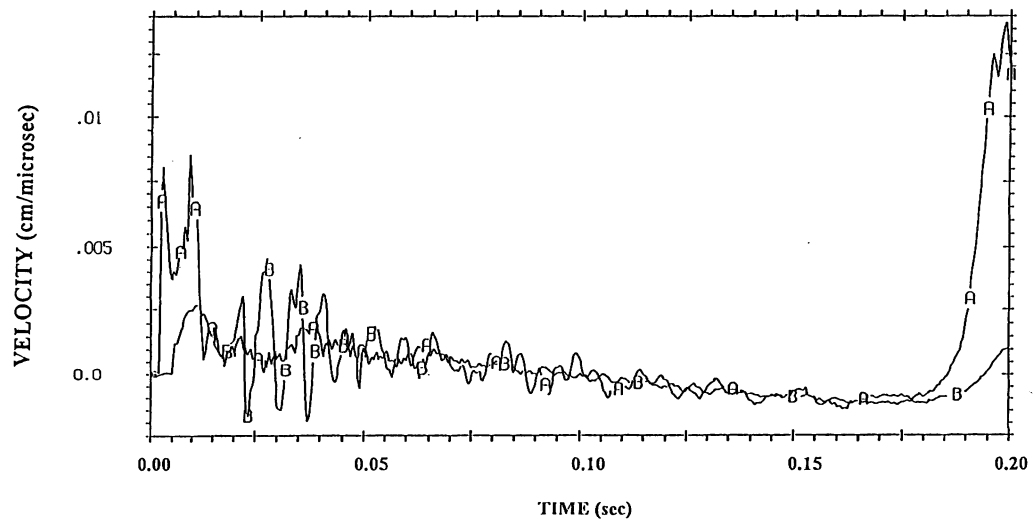

FIGURE 13 Time histories of shell velocities, A designates the front apex and B the rear apex.

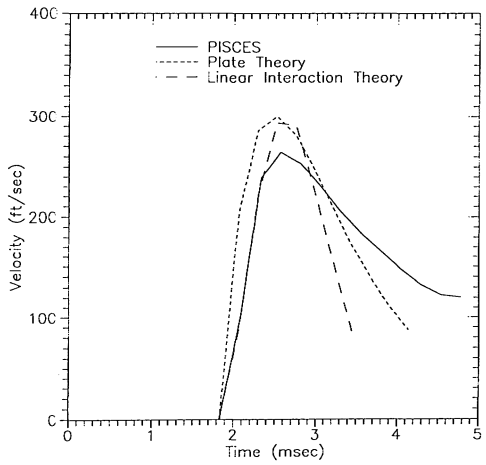

FIGURE 14 Comparison of results for the early time velocity of the shell apex facing the explosion.

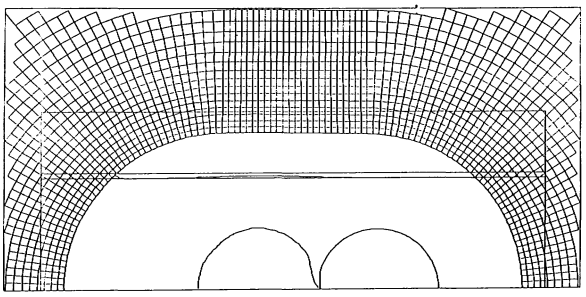

FIGURE 15 Shape of the bubble attaching to the steel shell at 0.060 s.

ucts, the numerical results indicate in Fig. 16 that this bubble also attains the same maximum volume as the previous fixed sphere case at $t = 0.093$ s but contracts to its minimum volume at $t = 0.193$ s, 0.006 s earlier than the fixed sphere case. Figure 17 portrays the bubble near its maximum size and indicates that the bubble still intersects only a small area of the shell surface with a protruding part. Again, the pressure inside the bubble then has fallen substantially below the ambient and except for a small part contacting the shell, the bubble is being pushed back by the surrounding water at most of its surface. The flow field associated with the contracting bubble and the intersection by the bubble cause an imbalance in pressure between the two sides of the opposite apexes and the shell thus is pushed back toward the explosion center as can be also seen from the time histories of the shell displacement in Fig. 12. Figure 18 shows that the contracting bubble has detached from the shell. Figure 19 portrays the bubble and the shell at $t = 0.180$ s and reveals that the contracting bubble then assumes a pear shape with a dimple formed facing the shell. Figure 20 portrays the bubble at $t = 0.190$ s near its minimum and the numerical results indicate that no bubble jet has been formed in sharp contrast to the previous fixed sphere case. Therefore, the bubble loading on this spherical shell is due to the bubble pulse only and is much different from that on the previous fixed sphere. Figure 21 shows that at $t = 0.200$ s the bubble reexpands with an irregular shape and that the bubble pulse results

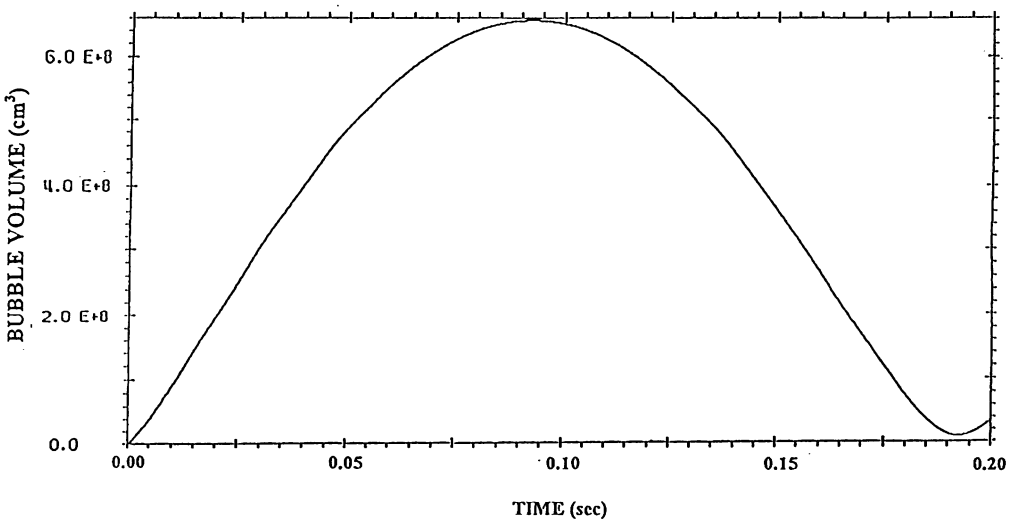

FIGURE 16 Time history of the volume of the bubble interacting with the steel shell.

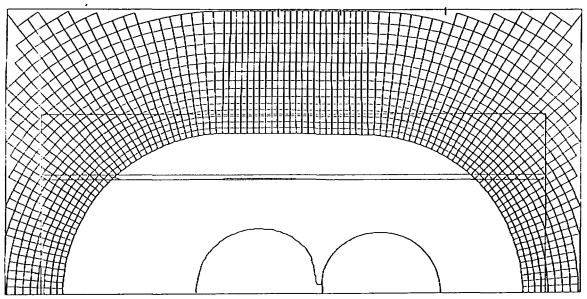

FIGURE 17 Shape of the bubble interacting with the steel shell at 0.100 s.

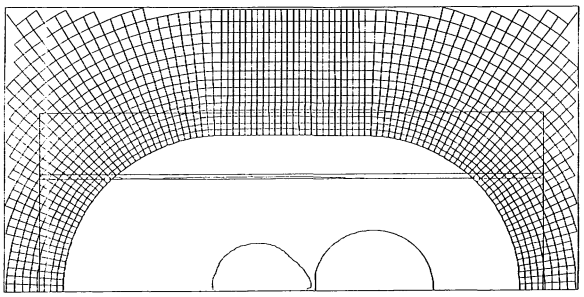

FIGURE 18 Detaching of the bubble from the steel shell at 0.160 s.

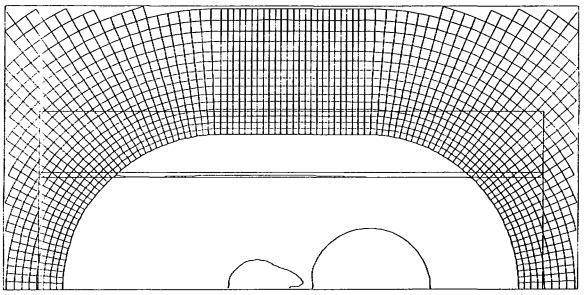

FIGURE 19 Contracting bubble shape and shell deformation at 0.180 s.

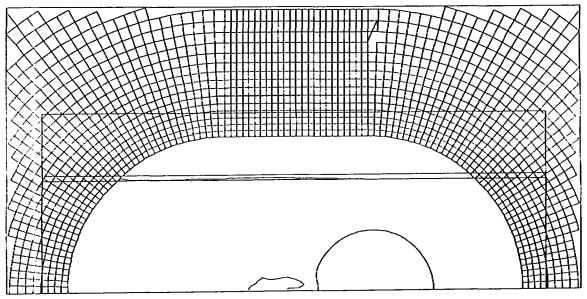

FIGURE 20 Contacting bubble shape and shell deformation at 0.190 s.

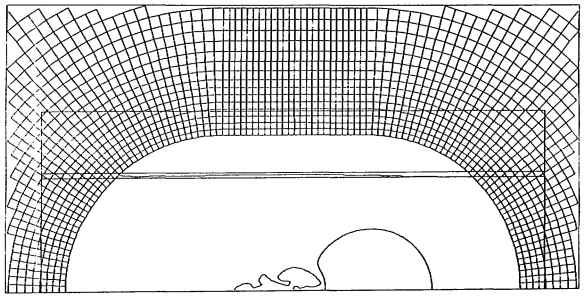

FIGURE 21 Reexpanding bubble shape and shell deformation at 0.200 s.

in a large shell deformation that can also be correlated with the time histories of the shell deflections and velocities in Figs. 12 and 13, respectively. At $t = 0.200$ s, the shell deflection at the frontal apex has increased to 1.34 m (52.76 in.).

CONCLUSIONS

The PISCES 2DELK coupled Eulerian–Lagrangian computation method is very well suited for this type of problem. Its second-order accurate advection scheme in the Eulerian computation is capable of correctly tracking the surface of the pulsating bubble. By juxtaposing the results for the fixed sphere case and the unrestrained steel spherical shell case, it is shown that the shell response motion could be a significant factor in determining the characteristics of the flow field surrounding a nearby pulsating bubble and consequently strongly influences the manner of collapse of the bubble, the formation of the bubble jet, and the bubble pulsation period. This in turn will strongly influence the characteristics of the bubble loading on the structure. Therefore, to rigorously analyze the response of the structure, the interaction among the initial shock wave, the structure, its surrounding media and the explosion bubble need to be considered.

REFERENCES

Cole, R. H., 1948, *Underwater Explosion, Princeton University Press, Princeton, NJ.*

Dobratz, B. M., 1981, *LLNL Explosive Handbook,* UCRL-52997, Lawrence Livermore National Laboratory, Livermore, CA.

Geers, T. L., 1975, "Transient Response Analysis of Submerged Structures," in T. Belytschko, J. R. Osias, and P. V. Marcel, *Finite Element Analysis of*

Transient Nonlinear Structural Behavior, AMD-Vol. 14, ASME, New York, pp. 59–84.

Hancock, S., 1987, *PISCES 2DELK Theoretical Manual,* PISCES International bv, San Leandro, CA.

Hicks, A. N., 1986, "Explosion Induced Whipping," in C. S. Smith and J. D. Clarke, *Advances in Marine Structures,* Elsevier Applied Science Publishers, Ltd., London and New York, pp. 390–410.

Huang, H., Lu, Y. P., and Wang, Y. F., 1971, "Transient Interaction of Spherical Acoustic Waves and a Spherical Elastic Shell," *Journal of Applied Mechanics,* Vol. 38, pp. 71–74.

Johnson, G. R., and Cook, W. H., 1983, "A Constitutive Model and Data for Metals Subjected to Large Strains, High Strain Rates, and High Temperatures," in *Proceedings of the 7th International Symposium on Ballistics,* The Hague, The Netherlands, pp. 541–554.

Keil, A. H., 1961, "The Response of Ships to Underwater Explosions," Paper no. 7 presented at the Annual Meeting of the Society of Naval Architects and Marine Engineers, New York, November 16–17.

Plesset, M. S., and Chapman, R. B., 1971, "Collapse of an Initially Spherical Vapour Cavity in the Neighbourhood of a Solid Boundary," *Journal of Fluid Mechanics,* Vol. 47, pp. 283–290.

Snay, H. G., Hydrodynamics of Underwater Explosions," in *Symposium on Naval Hydrodynamics,* 1957, Publication 515, National Academy of Science, National Research Council, Washington, DC, pp. 325–352.

Tipton, R. E., Steinberg, D. J., and Tomita Y., 1991, "Bubble Expansion and Collapse Near a Rigid Wall," UCRL-102945, Lawrence Livermore National Laboratory, Livermore, CA.